Original Research

MRI of Focal Nodular Hyperplasia (FNH) With Gadobenate Dimeglumine (Gd-BOPTA) and SPIO (Ferumoxides): An Intra-Individual Comparison

Luigi Grazioli, MD,[1]* Giovanni Morana, MD,[2] Miles A. Kirchin, PhD,[3] Paolo Caccia, MD,[1] Laura Romanini, MD,[1] Maria P. Bondioni, MD,[1] Carlo Procacci, MD,[2] and Antonio Chiesa, MD[1]

Purpose: To compare the efficacy of two different MR contrast agents for the detection and diagnosis of focal nodular hyperplasia (FNH).

Materials and Methods: Fifty patients with 83 FNH lesions detected on spiral CT were studied in two different MRI sessions with Gd-BOPTA (MultiHance®) and ferumoxides (Endorem®). MRI with Gd-BOPTA was performed precontrast (T1wGRE and T2wTSE sequences) and during the dynamic and late (1–3 hours) phases after injection (T1wGRE sequences only). MRI with ferumoxides (T1wGRE and T2wTSE sequences) was performed before and at least 30 minutes after injection. Hyper- or isointensity of FNH in the late phase was considered typical for Gd-BOPTA, while isointensity or lesion hypointensity was considered typical for ferumoxides.

Results: With Gd-BOPTA, 83 FNH lesions (100%) appeared hyperintense during the arterial phase of dynamic MRI. All but one lesion was iso- or slightly hyperintense in the portal-venous and equilibrium phases. In the late phase, 81 FNH lesions were hyper- or isointense to the surrounding parenchyma, with two lesions appearing slightly hypointense. With ferumoxides, a significant ($P < 0.001$) number (21/83, 25.3%) of FNH lesions (mean diameter = 16.8 ± 6.6 mm) were not visible. Of the visible FNH lesions, 38/62 were slightly hyperintense, and 24/62 were isointense to the surrounding parenchyma on the T2wTSE images. On the T1wGRE images, 42/62 lesions were isointense, 19/62 were slightly hyperintense, and one lesion was slightly hypointense. Seventeen lesions in 12 patients with previous neoplasia were all detected after Gd-BOPTA administration, whereas only nine of these 17 lesions (52.9%) were detected after ferumoxide administration. Two of these nine lesions showed atypical enhancement features.

Conclusion: Gd-BOPTA-enhanced MRI is significantly better than ferumoxide-enhanced MRI for the identification and characterization of FNH.

Key Words: focal nodular hyperplasia (FNH); MR imaging; MR contrast agents; gadobenate dimeglumine (GD-BOPTA); ferumoxides; superparamagnetic iron oxides (SPIOs)
J. Magn. Reson. Imaging 2003;17:593–602.

FOCAL NODULAR HYPERPLASIA (FNH) is a benign hypervascular hepatic lesion characterized by the presence of normal hepatocytes with a malformed biliary system (1). It is the result of a hyperplastic response to abnormal vasculature (2). Like hepatocellular adenoma, FNH occurs predominantly in women of child-bearing age who regularly use oral contraception. However, unlike adenoma, the use of oral contraception does not appear to be a causal factor in the formation of FNH (3,4). The ability to differentiate FNH from other benign lesions, such as adenoma, as well as from hypervascular malignant lesions such as breast cancer metastases, sarcoma, or carcinoid tumor, is of great clinical importance, particularly because atypical FNH lesions occur with comparatively high frequency in the adult population (5–9).

Until recently, contrast-enhanced MRI of the liver was performed using conventional gadolinium contrast agents. Efficacy with these agents relies on differential blood flow between the normal liver and the lesion (10). In recent years, however, a number of liver-specific MR contrast agents have become available. These agents can be broadly categorized as those targeted to Kupffer cells (i.e., superparamagnetic iron oxide (SPIO) particles, such as ferumoxides (Endorem®; Guerbet, Aulnay-sous-Bois, France)) (11,12) and those targeted to hepatocytes (e.g., Mn-DPDP (Mangafodipir; Amersham Health; Oslo, Norway)) (13). These liver-specific agents differ from the conventional gadolinium-based agents in that imaging can only be performed in a delayed phase after administration of the contrast agent, when accumulation of the contrast agent in the target cells has already occurred (12,13).

[1]Department of Radiology, University of Brescia, Brescia, Italy.
[2]Department of Radiology, University of Verona, Verona, Italy.
[3]Worldwide Medical Affairs, Bracco Imaging SpA, Milan, Italy.
Presented at the 10th Annual Meeting of ISMRM, Honolulu, 2002.
*Address reprint requests to: L.G., Department of Radiology, University of Brescia, Ple. Spedali Civili 1, 25100 Brescia, Italy.
E-mail: lgrazioli@yahoo.com
Received July 29, 2002; Accepted January 13, 2003.
DOI 10.1002/jmri.10289
Published online in Wiley InterScience (www.interscience.wiley.com).

Another contrast agent with liver-specific properties is Gd-BOPTA (gadobenate dimeglumine MultiHance®; Bracco Imaging SpA, Milano, Italy) (14). In common with SPIOs and Mn-DPDP, Gd-BOPTA can be used in conjunction with delayed-phase imaging (generally at 1–3 hours postinjection) to improve the detection and characterization of focal liver lesions (15–17). However, Gd-BOPTA differs from SPIOs and Mn-DPDP in that dynamic-phase imaging can still be performed in a manner analogous to that employed for conventional gadolinium-based agents (18–20).

Recently, the value of Gd-BOPTA in dynamic- and delayed-phase imaging of typical and atypical FNH was reported (21). The purpose of the present study was to compare Gd-BOPTA and SPIOs (ferumoxides) intra-individually for their use in identifying and characterizing FNH.

MATERIALS AND METHODS

Subjects

A total of 50 patients (44 females and six males; mean age 38.9 ± 10.8 years; range 22–65 years) were studied between March 1999 and April 2002. The patients all underwent an initial spiral CT examination of the liver, which revealed a total of 83 lesions. Histology results subsequent to lesion biopsy were available for 50 lesions in 35 patients. For patients with multiple lesions, histologic assessment was performed for at least two of the most representative lesions. The remaining 15 patients underwent follow-up for at least 1 year. No significant variations in lesion size or morphology were noted in these patients, and the imaging characteristics revealed by other imaging modalities (multiphase spiral CT [$N = 15$], scintigraphy with HIDA [$N = 3$], and MRI with conventional Gd chelate [Gd-DTPA; $N = 3$]) were typical of FNH.

Of the 50 patients enrolled in the study, 27 presented with nonspecific symptoms—principally pain in the superior abdominal quadrants. The remaining patients were asymptomatic, and the detection of lesions was incidental. Twenty-five of the 44 female patients had used oral contraceptives for at least 1 year, and 12 patients overall were known to have previous neoplasia (sarcoma, $N = 1$; pulmonary carcinoid, $N = 1$; melanoma, $N = 2$; uterine cancer, $N = 1$; renal cancer, $N = 2$; and breast cancer, $N = 5$). In the 12 patients with previous neoplasia, a total of 17 hypervascular liver lesions were detected on preliminary spiral CT examination. Lesion biopsies were performed on at least one lesion in each of these patients. One patient with five lesions had preexisting hepatopathy (hepatitis C). Two of these lesions were biopsied, and follow-up was performed for 14 months.

MRI

Each patient underwent MRI in two different sessions on a 1.5 Tesla superconducting imager (Symphony; Siemens, Erlangen, Germany) using a phased-array torso multicoil. In the first examination, the patients received 15 μmol Fe/kg bodyweight ferumoxides (Endorem®; Guerbet, Aulnay-sous-Bois, France) by slow (10 mL/minute) intravenous infusion. In the second examination, the patients received 0.1 mmol/kg bodyweight Gd-BOPTA (gadobenate dimeglumine (MultiHance®; Bracco Imaging SpA, Milano, Italy)) by bolus (≥2 mL/second) intravenous injection.

MRI with ferumoxides was performed before contrast infusion and at least 30 minutes after infusion. T2-weighted turbo spin-echo images (T2wTSE; TR/TE = 3900–4100/90–108 msec) and T1-weighted gradient-echo images (T1wGRE; TR/TE/FA = 110–140/4.8 msec/80°) were acquired both pre- and postcontrast. MRI with Gd-BOPTA was performed precontrast, during the dynamic phase of contrast enhancement at 20–30 seconds (arterial phase), 50–80 seconds (portal-venous phase), and 3–5 minutes (equilibrium phase) postinjection, and during the delayed phase at 1–3 hours postinjection. T1wGRE and T2wTSE images were acquired precontrast with repetition of the T1wGRE sequence during each of the postcontrast phases of enhancement. The imaging parameters employed were identical to those used with ferumoxides. The slice thickness varied between 5 and 8 mm depending on the hepatic volume imaged, but was kept constant for each patient. The entire liver was imaged in a single acquisition during a single breath-hold.

A mean intervening period of approximately 3 months (minimum = 1 week; maximum = 14 months) was allowed between the MR examinations with ferumoxides and Gd-BOPTA. During this period no patient developed hepatopathy, and no significant variations in lesion size or morphology were noted. It was therefore assumed that the intervening period did not influence the enhancement characteristics of the lesions or liver parenchyma on postcontrast images.

Image Assessment

The criteria for image assessment were based on published findings and on experience gained over several years of using Gd-BOPTA and ferumoxides in routine clinical practice. Typical features of FNH on unenhanced MR images and on MR images after Gd-BOPTA and ferumoxides administration are shown in Figure 1. On the unenhanced images, typical FNH demonstrated homogenous iso- or slight hypointensity to the normal liver parenchyma on T1-weighted sequences, and homogenous iso- or slight hyperintensity on T2-weighted sequences. The typical enhancement pattern seen on dynamic-phase images after rapid bolus injection of Gd-BOPTA was similar to that observed after bolus injection of other gadolinium agents, i.e., an initial marked homogenous hyperintensity on T1-weighted images during the arterial phase at 20–30 seconds postinjection, with subsequent rapid washout during the portal-venous and equilibrium phases at 60–80 seconds and 3–5 minutes postinjection, respectively (6,22). Typical FNH on delayed-phase images after Gd-BOPTA injection demonstrated homogenous or heterogenous iso- or hyperintensity to the normal liver parenchyma (21).

The typical MRI feature of FNH on T2-weighted images after ferumoxide administration was a marked homogenous or heterogenous reduction of signal intensity

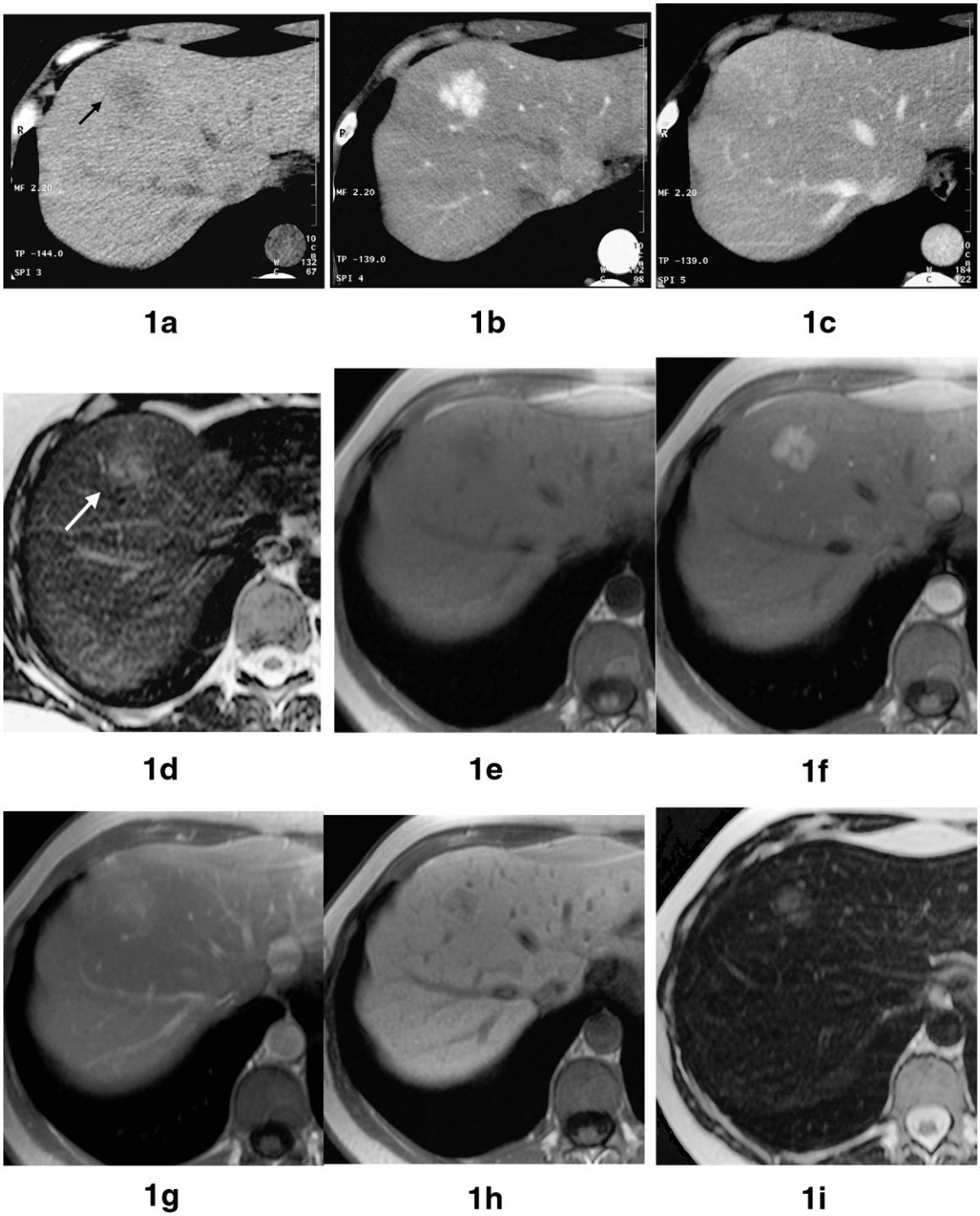

Figure 1. A case of typical FNH in a 37-year-old asymptomatic woman with a history of more than 10 years of oral contraceptive use. **a:** A local diffuse hypointense area (arrow) is visible in liver segment VIII on precontrast spiral CT images. The lesion demonstrates intense homogenous enhancement during (**b**) the arterial phase, and isointensity with the surrounding parenchyma on (**c**) subsequent portal venous phase images. MRI reveals a diffuse and poorly delineated hyperintense lesion (arrow) on (**d**) unenhanced T2wTSE sequences (TR = 3900, TE = 98), which appears hypointense against the surrounding parenchyma on (**e**) unenhanced T1wGRE sequences (TR = 140, TE = 4.8, FA = 80°). **f:** During the arterial phase (25 seconds) after administration of Gd-BOPTA, the lesion demonstrates intense homogenous enhancement while the central scar remains hypointense. **g:** Rapid contrast wash-out by the time of the subsequent portal venous phase (70 seconds) image leaves the lesion isointense against the surrounding parenchyma, with the central scar appearing hyperintense. **h:** On images acquired at 3 hours postinjection, the lesion appears isointense, with a hyperintense peripheral rim and a hypointense central scar. **i:** On T2wTSE images (TR = 3900, TE = 98) acquired at 30 minutes after administration of ferumoxides, the lesion appears isointense to faintly hyperintense against the surrounding parenchyma.

Table 1
Detection of FNH on Unenhanced Images and Images Obtained After Administration of Gd-BOPTA and Ferumoxides

Signal intensity	Pre-contrast (Unenhanced) phase		Post-Gd-BOPTA				Post-ferumoxides	
			Dynamic phase			Delayed phase	Delayed phase	
	T2wTSE	T1wGRE	Arterial	Portal venous	Equilibrium	1–3 hours	T2wTSE	T1wGRE
Hyperintense	34	0	83	29	16	52	38	19
Isointense	22	27	0	44	50	18	24	42
Hypointense	1	27	0	1	1	2	0	1
Not visible	26	29	0	9	16	11	21	21
Total	83	83	83	83	83	83	83	83

compared to that seen on unenhanced T2-weighted images. Generally, FNH appeared isointense or slightly hypointense to the normal liver parenchyma on T2-weighted images after ferumoxide injection (23,24), although a faint hyperintense appearance was not considered atypical.

A typical feature of larger FNH nodules (generally > 30 mm) was the presence of a central scar (Fig. 1). Although atypical lesions lacking a central scar or with calcification are not uncommon (1,6,7), a frequent observation is the appearance of a hyperintense stellate area on T2-weighted images and a corresponding hypointense area on T1-weighted images during the arterial and portal-venous phases after Gd-BOPTA injection, followed by hyperintensity during the equilibrium phase (21). On delayed T1-weighted images after Gd-BOPTA administration, the central scar was considered typical if it appeared as a hypointense stellate area.

The signal intensity of the central scar on postcontrast images after ferumoxide administration is typically unchanged compared to that on unenhanced images (23).

Images were evaluated qualitatively by two equally-experienced radiologists in terms of the number and size of lesions present, and their enhancement characteristics relative to findings on preliminary spiral CT examination. The locations of all lesions detected during each imaging session were recorded on segmental liver maps (25) for subsequent correlation with the results of the other imaging session. Discordant cases ($N = 4$) on image evaluation were resolved by consensus.

Statistical Analysis

The results of the study were statistically evaluated by the use of McNemar's test for independent proportions. Structural zeros in the 2×2 contingency tables were avoided by inputting 0.5.

RESULTS

Table 1 shows the numbers of lesions detected on unenhanced images and on enhanced images after ferumoxide and Gd-BOPTA administration, and the enhancement patterns observed.

Lesion Detection

A total of 57 lesions were detected on unenhanced MRI (T1- and T2-weighted images combined) before both Gd-BOPTA and ferumoxide examinations. Thus, 26 (31.3%) of the 83 lesions seen on preliminary spiral CT were not seen on unenhanced MRI. The lesions detected on unenhanced images during the ferumoxide examination were the same as those detected on unenhanced images during the Gd-BOPTA examination.

An increased number of lesions were detected on postcontrast MR images. On dynamic T1wGRE images acquired after injection of Gd-BOPTA, a total of 83 lesions were detected. For 48/50 patients (96%) the lesions detected on MR images after Gd-BOPTA administration were the same as those seen on spiral CT. The two discordant patients (one patient with one lesion less on Gd-BOPTA-enhanced MRI, and one patient with one lesion more on Gd-BOPTA-enhanced MRI) each had multiple lesions. The mean size of the 83 lesions detected on MR images after Gd-BOPTA was 34.1 ± 23.2 mm (range: 6–100 mm).

A total of 62 lesions (i.e., five more than on the unenhanced images) were detected on MR images (T2wTSE and T1wGRE combined) acquired after ferumoxide administration. The mean size of the 62 lesions detected on images acquired after ferumoxide administration was 40.8 ± 24.2 mm (range: 10–100 mm). The 21 lesions (25.3%) seen on images acquired after Gd-BOPTA injection, but not seen on any images after ferumoxide injection, were generally small FNH lesions with a mean diameter of 16.8 ± 6.6 mm (range: 6–30 mm). Figure 2 shows an example of an FNH lesion seen on images after Gd-BOPTA administration but not on images after ferumoxide administration.

Statistical evaluation revealed that significantly more FNH lesions were detected on dynamic- and delayed-phase images after Gd-BOPTA administration than on delayed images after ferumoxide injection ($P < 0.001$ for the comparison of lesions detected on dynamic images after Gd-BOPTA vs. postcontrast images after ferumoxides; $P = 0.002$ for the comparison of lesions detected on delayed-phase images only after Gd-BOPTA vs. postcontrast images after ferumoxides). Similar results were obtained for the detection of lesions < 3 cm in size (51 small lesions detected on dynamic images after Gd-BOPTA compared with only 30 lesions detected after ferumoxides; $P < 0.001$).

The 17 lesions detected on spiral CT in the 12 patients with previous neoplasia consisted of one lesion in the patient with sarcoma, one lesion in the patient with uterine cancer, two lesions in the patient with pulmonary carcinoid, six lesions in two patients with renal

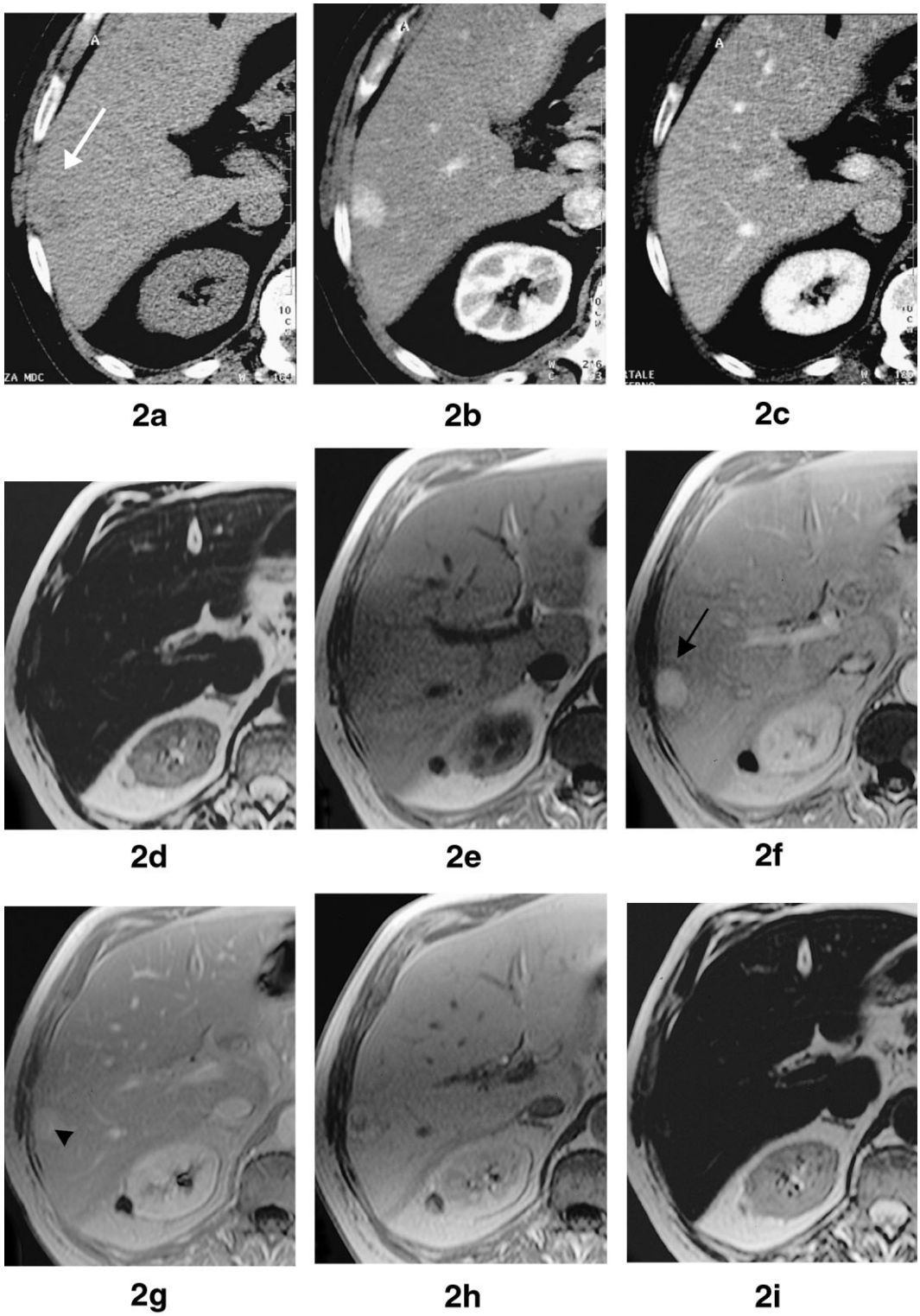

Figure 2. FNH in a 78-year-old patient with melanoma. **a:** A diffuse, faintly hypointense area (arrow) is visible in liver segment VI on precontrast spiral CT images. On postcontrast images during the (**b**) arterial and (**c**) portal venous phases the lesion demonstrates first an intense homogenous enhancement and then isointensity with the surrounding parenchyma. The lesion cannot be seen on unenhanced (**d**) T2wTSE (TR = 3900, TE = 98) or (**e**) T1wGRE (TR = 140, TE = 4.8, FA = 80°) MR images. **f:** During the arterial phase (25 seconds) after administration of Gd-BOPTA, the lesion (arrow) demonstrates intense homogenous enhancement, although no central scar is visible. **g:** On the portal venous phase (70 seconds) images the lesion is apparent as a homogenous, faintly hyperintense nodule with a hyperintense central scar (arrowhead). **h:** At 3 hours after Gd-BOPTA administration the lesion is visible as a hyperintense mass with a markedly hypointense central scar. The hyperintense appearance of the lesion reflects abnormal biliary drainage. **i:** No lesion can be seen on T2wTSE images (TR = 3900, TE = 98) acquired at 30 minutes after administration of ferumoxides.

cancer (five lesions in one patient, one lesion in the other), one lesion in each of the two patients with melanoma, and one lesion in each of the five patients with breast cancer. All of these lesions were detected on dynamic MR images acquired after Gd-BOPTA injection. In contrast, only nine of these 17 lesions (52.9%) were detected on postcontrast images (T2wTSE and T1wGRE images combined) after ferumoxide administration. Eight of the 17 lesions in five of the 12 patients with previous neoplasia were not visible on postcontrast images after ferumoxide administration. These eight lesions consisted of four of the five lesions detected in one of the patients with previous renal cancer, two lesions in two patients with breast cancer, one lesion in the patient with sarcoma, and one lesion in one of the patients with melanoma (Fig. 2).

Lesion Enhancement

On dynamic-phase imaging after Gd-BOPTA administration, 81 of the 83 detected lesions (97.6%) appeared homogenously hyperintense to the background normal liver parenchyma at 20–30 seconds postinjection, and iso- or slightly hyperintense at 60–80 seconds and 3–5 minutes postinjection. Two lesions in two patients appeared heterogenously hyperintense at 20–30 seconds postinjection. In one patient this was due to areas of hemorrhage within the lesion, and in the other patient a solitary lesion of 100 mm had a nodular appearance with varying enhancement from one nodule to the next.

Of the 83 lesions seen on dynamic-phase imaging, 52/83 lesions (62.7%) were also hyperintense against the background normal liver parenchyma on delayed-phase images. The remaining 31 lesions were either isointense (18/83 lesions, 21.7%), atypically hypointense (2/83 lesions, 2.4%), or not visible (11/83 lesions, 13.3%). The enhancement pattern of the 72 lesions seen on delayed images was judged to be homogenous in 50 cases (69.4%), heterogenous in 15 cases (20.8%), and peripherical in seven cases (9.7%). Of the two heterogenously hyperintense lesions on dynamic-phase images, one lesion appeared homogenously hyperintense on delayed-phase images and the other was heterogenously hyperintense. Of the 17 lesions detected after Gd-BOPTA injection in patients with previous neoplasia, nine lesions appeared isointense and eight lesions were hyperintense to the normal liver parenchyma. The eight hyperintense lesions comprised four lesions that were homogenously hyperintense and four lesions that were heterogenously hyperintense with a mainly peripheral enhancement.

On T2wTSE images after ferumoxide administration, 38/62 visible lesions (61.3%) were hyperintense and the remainder (24/62 lesions, 38.7%) were isointense to the background normal liver parenchyma. On T1wGRE images after ferumoxide administration, 19/62 visible lesions (30.6%) were hyperintense. A further 42/62 lesions (67.7%) were isointense or slightly hyperintense, while one single lesion appeared hypointense to the normal background parenchyma. Overall, typical behavior (homogenous or heterogenous decrease of signal intensity following ferumoxides) was noted for 42 lesions, and atypical behavior was observed for 20 lesions (32.3%) (Fig. 3).

Of the nine lesions detected after ferumoxide injection in patients with previous neoplasia, two lesions in two patients were considered atypical due to a hyperintense appearance on postcontrast T1wGRE images and both pre- and postcontrast T2wTSE images (Fig. 4).

A central scar (Table 2) was seen as a hypointense area in 29/83 lesions, and as a hyperintense area in 4/83 lesions on T1wGRE images during the arterial phase after Gd-BOPTA administration. By the equilibrium phase of contrast enhancement, all but two of the hypointense scars had become either hyperintense (N = 25) or isointense (N = 2), while the four hyperintense scars remained hyperintense. One further scar was evident as a hyperintense area during the equilibrium phase that had not been seen on any of the earlier phases. On delayed-phase images after Gd-BOPTA, central scars were visible in 35/83 (42.2%) detected lesions (mean lesion size: 45.4 ± 23.6 mm)—in each case as a hypointense area. Hypointense scars were seen in four of the 17 lesions detected with Gd-BOPTA on delayed-phase images in patients with previous neoplasia. In contrast, central scars were seen in only two of these four lesions on precontrast and dynamic-phase images after Gd-BOPTA administration.

On ferumoxide-enhanced images, central scars were visible on T2wTSE images as hyperintense areas in 17/62 (27.4%) detected lesions (mean lesion size: 51.3 ± 23.8 mm) and on T1wGRE images as hypointense areas in 14/62 (22.6%) detected lesions (mean lesion size: 56.8 ± 22.5 mm). The three scars seen on T2wTSE images but not on T1wGRE images were each present in small lesions (20–32 mm). Overall, significantly more central scars were detected on Gd-BOPTA-enhanced images than on ferumoxide-enhanced images ($P < 0.001$ for comparisons of scars detected on dynamic images after Gd-BOPTA vs. postcontrast images after ferumoxides, and on delayed images after Gd-BOPTA vs. postcontrast images after ferumoxides). Among the nine lesions detected with ferumoxides in patients with previous neoplasia, central scars were observed as hyperintense areas in just two lesions on T2wTSE images, and in no lesions on T1wGRE images.

DISCUSSION

Characterization of disease commences once an abnormality is found. An imaging procedure that can detect liver masses should also be able to at least differentiate between benign and malignant lesions. In recent years, the importance of this dual imaging goal has been highlighted by the recognition of an unexpectedly high prevalence of benign liver tumors in the adult population. In the vast majority of cases, these are nonsolid lesions, such as small cavernous hemangiomas and cysts that do not require treatment (26).

Initial reports on the use of MRI to differentiate between nonsolid hemangiomas and solid primary and secondary hepatic malignancies demonstrated the usefulness of comparing signal intensities on heavily T2-weighted images (27–29). Specifically, a smooth homogenous "light bulb" pattern was found to be more

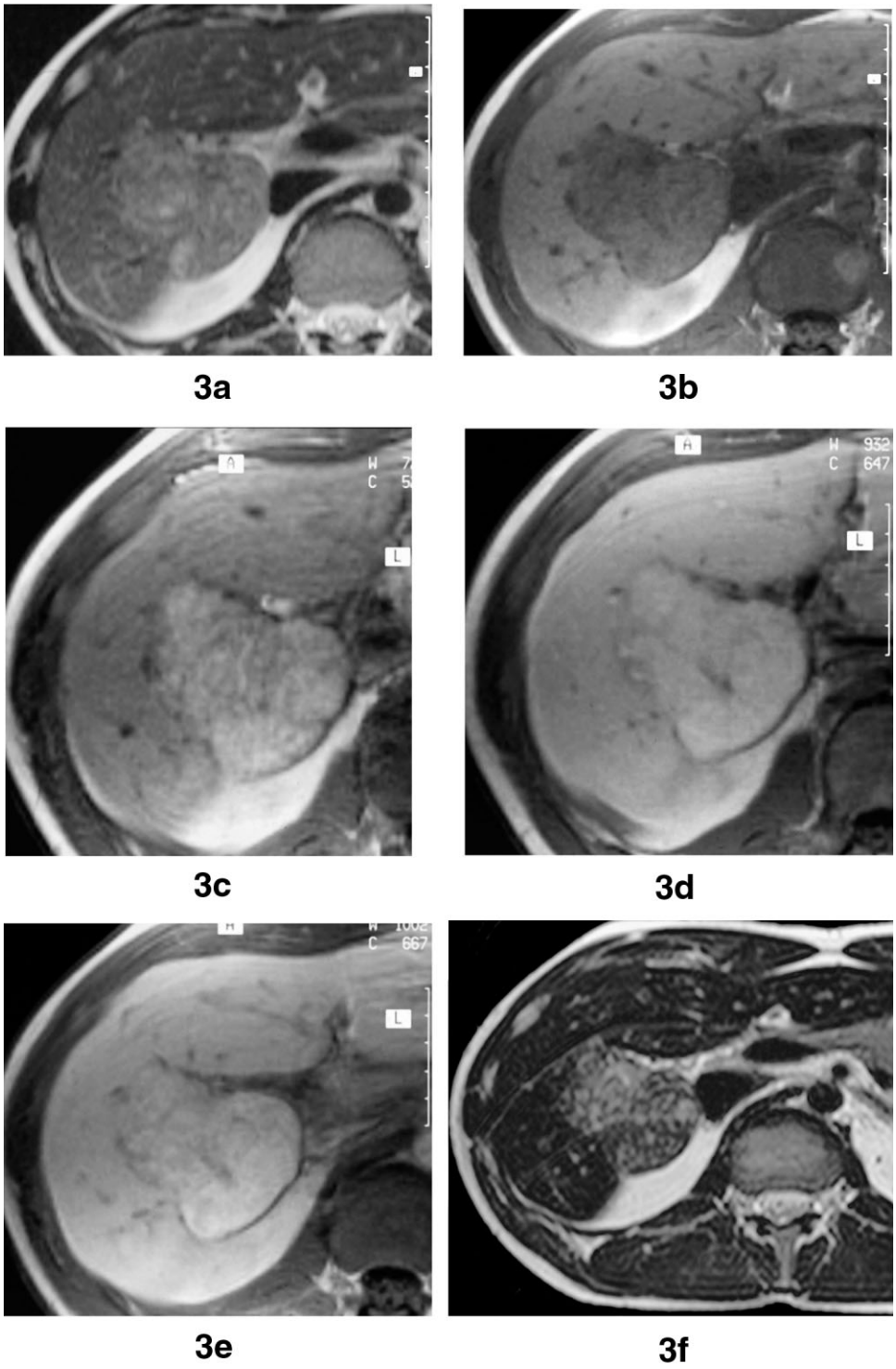

Figure 3. FNH in a 31-year-old male patient with chronic pain in his left side. Unenhanced (**a**) T2wTSE and (**b**) T1wGRE MR images reveal a large, structurally inhomogenous lobular lesion in segment VI. T1wGRE images acquired during (**c**) the arterial phase (25 seconds) after administration of Gd-BOPTA reveals marked inhomogenous enhancement of the nodule, which persists into (**d**) the portal venous phase (70 seconds). A hypointense central scar is clearly visible on the portal venous phase image. **e:** At 3 hours after the administration of Gd-BOPTA, the lesion is still hyperintense to the surrounding parenchyma and the central scar is still clearly hypointense. **f:** On T2wTSE images (TR = 3900, TE = 98) acquired at 30 minutes after administration of ferumoxides, the lesion is apparent as a inhomogenous hyperintense mass with mottled areas of isointensity.

suggestive of hemangiomas or cysts, while indistinct margins and rim, target, or doughnut appearances were described as being more indicative of malignancy (28,29). Later studies reported that the rapid (bolus) administration of extracellular fluid agents like Gd-DTPA or gadoteridol, coupled with fast or ultrafast dynamic MRI, can allow better assessment of lesion hemodynamics, and thus provide diagnostic clues that are independent of and additive to those obtained with nonenhanced MRI (30–33).

After hemangiomas, FNH lesions are the second most common lesions of the liver. They are present in 3%–5% of the population, mainly in women of child-bearing age (34). The advent of spiral CT and dynamic MRI has led to increased detection of these lesions, particularly those of smaller size (<15 mm). With the availability of spiral CT, the rate of detection of FNH in our department has increased by almost 30% over the past 3 years. The dynamic enhancement pattern is useful not only for detection, but also for characterization. In this

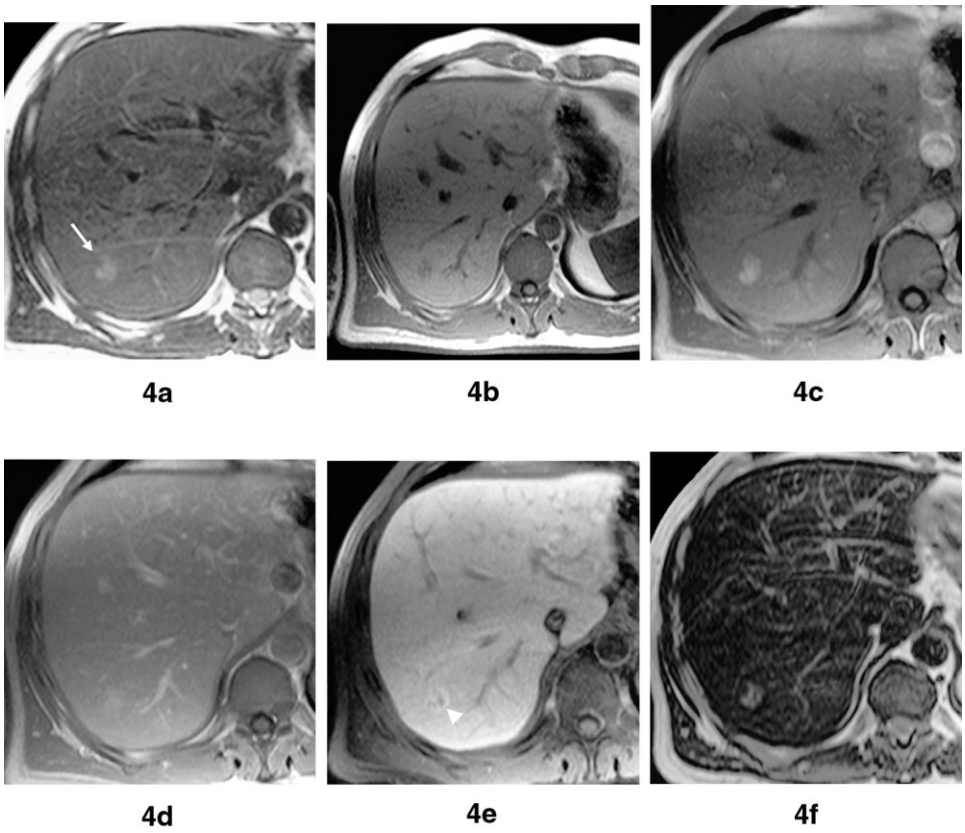

Figure 4. FNH in a 37-year-old male patient undergoing follow-up 2 years after surgery for renal carcinoma. **a:** The unenhanced T2wTSE image reveals a small, diffuse, poorly delineated hyperintense lesion (arrow) in segment VII. **b:** On the unenhanced T1wGRE image the lesion appears hypointense to the surrounding parenchyma. T1wGRE images acquired during the (**c**) arterial (25 seconds) and (**d**) subsequent portal venous (70 seconds) after phases the administration of Gd-BOPTA reveal an enhancement pattern typical of FNH: intense homogenous enhancement followed by rapid contrast wash-out to leave the lesion isointense to the surrounding parenchyma. **e:** On T1wGRE images acquired at 3 hours after the administration of Gd-BOPTA, the lesion reveals characteristic hyperintensity with a hypointense central scar (arrowhead). **f:** On T2wTSE images acquired at 30 minutes after the administration of ferumoxides, the lesion is clearly visible as a hyperintense mass. This appearance reflects the lack of uptake of SPIO particles by the FNH nodule, and could easily be mistaken for metastatic cancer.

regard, an intense and homogenous enhancement during the arterial phase, followed by rapid and homogenous wash-out during the portal-venous and equilibrium phases, is important for the characterization of FNH, as is the presence of a hyperintense, stellate central scar on equilibrium-phase images. Unfortunately, 20%–50% of FNH lesions show an atypical appearance on spiral CT, and thus in a large percentage of cases a definitive diagnosis is not achievable (1,3,7,35,36). Contrast-enhanced, dynamic-phase MRI using traditional extracellularly-distributed, gadolinium-based contrast agents provides the greatest diagnostic sensitivity among the techniques in current use, particularly when combined with the information available on unenhanced T1- and T2-weighted images (22). Nevertheless, even with this imaging modality, the presence of atypical features may prevent accurate characterization of FNH in some cases. Furthermore, diagnosis on

Table 2
Detection of FNH Central Scar on Unenhanced Images and Images Obtained After Administration of Gd-BOPTA and Ferumoxides

Signal intensity	Pre-contrast (Unenhanced phase)		Post-Gd-BOPTA				Post-ferumoxides	
			Dynamic phase			Delayed phase	Delayed phase	
	T2wTSE	T1wGRE	Arterial	Portal venous	Equilibrium	1–3 hours	T2wTSE	T1wGRE
Hyperintense	23	0	4	6	30	0	17	0
Isointense	0	0	0	4	2	0	0	0
Hypointense	0	27	29	24	2	35	0	14
Not visible	60	56	50	49	49	48	66	69
Total	83	83	83	83	83	83	83	83

dynamic phase MRI relies on the same morphologic and hemodynamic features as spiral CT.

Abnormal biliary drainage is the most important and constant pathologic feature of FNH (1). This feature is very useful for differentiating these pseudo-tumoral masses which generally do not require surgical intervention, from benign hepatocellular adenomas which frequently are referred for surgical resection because of their high tendancy for hemorrhage and malignant degeneration (37). Neither spiral CT nor MRI with conventional contrast agents is effective at demonstrating this functional abnormality, although radionuclide imaging with tracers (such as technetium Tc 99m diethyl-iminodiacetic acid) that simulate the behavior of bilirubin may reveal the uptake and delayed excretion in FNH as a "hot spot" (1). FNH contains Kupffer cells in variable amounts. With SPIO-based contrast agents, which are taken up by Kupffer cells, a homogenous or heterogenous signal drop on T2-weighted images has been shown to represent additional functional information for characterization (38). However, Kupffer cells may be present in comparatively small numbers, and thus there is frequently insufficient signal drop after SPIO administration for the accurate identification of FNH. Furthermore, some lesions that lack Kupffer cells, including hemangioma and adenoma, have also been reported to demonstrate signal drop after SPIO administration. This appears to be due to pooling of the contrast agent within the vascular pools and peliosis-like dilatated vessels, which characterizes hemangiomas and adenomas, respectively (12). Finally, Kupffer cells may also be present in variable amounts in other benign lesions, such as regenerative nodular hyperplasia, as well as in malignant focal liver lesions, such as well-differentiated HCC (39). These lesions may thus show a signal intensity reduction similar to that observed for FNH, which would make it difficult to obtain an accurate diagnosis.

Gd-BOPTA is a paramagnetic, gadolinium-based contrast agent that behaves in a manner analogous to that of other gadolinium agents during the vascular-interstitial phase in the first minutes after injection, and as an agent with liver-specific properties in a later delayed phase (14,16). Thus, Gd-BOPTA is as effective for detecting lesions as conventional gadolinium agents during dynamic-phase imaging, but thereafter accumulates selectively in hepatocytes, which enables additional functional information to be acquired. In FNH, there is prolonged and excessive hepatocellular accumulation of the contrast agent because FNH lacks a well-formed bile canalicular system for normal excretion (1). This behavior is distinct from that seen in adenomas, which do not show significant uptake during the delayed phase (21). Thus, the use of Gd-BOPTA permits both morphologic and functional information to be obtained, with the advantage of greater spatial resolution than that achievable with nuclear scintigraphy.

The results of the present intra-individual comparative study indicate that Gd-BOPTA is significantly ($P < 0.001$) superior to ferumoxides for the identification and characterization of FNH. Only 62/83 lesions (74.7%) were identified during the MR examination with ferumoxides, and of these 62 lesions, 57 were identified on the unenhanced images alone. Ferumoxides contributed to the identification of only five additional lesions. As regards enhancement characteristics, these were considered typical for just 42 (67.7% (50.6% of the overall lesion population)) of the 62 lesions identified. During the MR examination with Gd-BOPTA a total of 83 lesions were identified, of which 26 were not seen on unenhanced MRI. The lesions identified comprised 82/83 lesions seen previously on spiral CT, plus one additional lesion not seen on spiral CT. All of these lesions (100%) demonstrated typical enhancement characteristics during the dynamic phase of contrast enhancement, while 81/83 lesions (97.6%) were typically hyperintense or isointense to the normal background liver parenchyma on delayed-phase images.

A recent study aimed at evaluating Gd-BOPTA for contrast-enhanced MRI of FNH revealed that a combination of dynamic- and delayed-phase images enables both morphologic and functional information to be acquired (21). Notably, the information available on delayed images was shown to allow the accurate characterization of 21/100 FNH lesions that were otherwise considered to have atypical features at dynamic-phase MR and other imaging modalities (21). The conclusion of this earlier study was that the ability to carry out dynamic- and delayed-phase imaging in clinical practice may be highly beneficial for both the detection and differential diagnosis of liver lesions—particularly small lesions in patients with a previous cancer, such as breast cancer, sarcoma, or carcinoid tumor. In the present study, 17 lesions in 12 patients with previous neoplasia demonstrated typical dynamic and delayed enhancement patterns, and were correctly diagnosed as FNH following Gd-BOPTA. Conversely, only nine of these 17 nodules were seen following ferumoxide administration. The remaining eight nodules in five patients were not seen, due to an uptake of ferumoxides similar to that taking place in normal surrounding parenchyma. However, because areas of hyperintensity indicative of a lack of ferumoxide uptake, and hence a lack of Kupffer cells, were not seen in these patients, it could be concluded that malignant lesions were not present. For these five patients, the inference was therefore not that benign nodules of FNH *were* present, but rather that malignant lesions were *not* present. On the other hand, of the nine lesions that were seen following ferumoxide injection, two lesions in two patients demonstrated a marked atypical hyperintense appearance. From a diagnostic standpoint, these lesions should be considered a greater cause for concern than the eight unseen lesions, because areas of hyperintensity following ferumoxide administration in patients with previous neoplasia could easily be confused with metastatic disease.

In conclusion, the results of this study suggest that Gd-BOPTA is a more appropriate contrast agent than ferumoxides for the identification and characterization of FNH. Further work is ongoing to evaluate these two agents in patients with other types of hepatocellular lesions, specifically hepatocellular carcinoma and hepatic adenoma.

REFERENCES

1. Boulahdour H, Cherqui D, Charlotte F, et al. The hot spot hepatobiliary scan in focal nodular hyperplasia. J Nucl Med 1993;34: 2105–2110.
2. Wanless IR, Mawdsley C, Adams R. On the pathogenesis of focal nodular hyperplasia of the liver. Hepatology 1985;5:1194–1200.
3. Cherqui D, Rahmouni A, Charlotte F, et al. Management of focal nodular hyperplasia and hepatocellular adenoma in young women: a series of 41 patients with clinical, radiological, and pathological correlations. Hepatology 1995;22:1674–1681.
4. Reddy KR, Kligerman S, Levi J, et al. Benign and solid tumors of the liver: relationship to sex, age, size of tumors and outcome. Am Surg 2001;67:173–178.
5. Bioulac-Sage P, Balabaud C, Wanlass IR. Diagnosis of focal nodular hyperplasia. Not so easy. Am J Surg Pathol 2001;25:1322–1325.
6. Mattison GR, Glazer GM, Quint LE, Francis IR, Bree RL, Ensminger WD. MR imaging of hepatic focal nodular hyperplasia: characterization and distinction from primary malignant hepatic tumors. AJR Am J Roentgenol 1987;148:711–715.
7. Caseiro-Alves F, Zins M, Mahfouz A-E, et al. Calcification in focal nodular hyperplasia: a new problem for differentiation from fibrolamellar hepatocellular carcinoma. Radiology 1996;198:889–892.
8. Welch TJ, Sheedy 2nd PF, Johnson CM, et al. Focal nodular hyperplasia and hepatic adenoma: comparison of angiography, CT, US, and scintigraphy. Radiology 1985;156:593–595.
9. Weimann A, Ringe B, Klempnauer J, et al. Benign liver tumors: differential diagnosis and indications for surgery. World J Surg 1997;21:983–990.
10. Saini S. Contrast-enhanced MR imaging of the liver. Radiology 1992;182:12–14.
11. Oudkerk M, van den Heuvel AG, Wielopolski PA, Schmitz PIM, Borel Rinkes IHM, Wiggers T. Hepatic lesions: detection with ferumoxide-enhanced T1-weighted MR imaging. Radiology 1997;203: 449–456.
12. Denys A, Arrive L, Servois V, et al. Hepatic tumors: detection and characterization at 1T MR imaging enhanced with AMI-25. Radiology 1994;193:665–669.
13. Kettritz U, Schlund JF, Wilbur K, Eisenberg LB, Semelka RC. Comparison of gadolinium chelates with manganese-DPDP for liver lesion detection and characterization: preliminary results. Magn Reson Imaging 1996;14:1185–1190.
14. Kirchin MA, Pirovano G, Spinazzi A. Gadobenate dimeglumine (Gd-BOPTA): an overview. Invest Radiol 1998;33:798–809.
15. Caudana R, Morana G, Pirovano G, et al. Focal malignant hepatic lesions: MR imaging enhanced with gadolinium benzyloxypropionictetra-acetate (BOPTA)—preliminary results of phase II clinical application. Radiology 1996;199:513–520.
16. Spinazzi A, Lorusso V, Pirovano G, Kirchin MA. Safety, tolerance, biodistribution and MR imaging enhancement of the liver with gadobenate dimeglumine. Acad Radiol 1999;6:282–291.
17. Grazioli L, Morana G, Caudana R, et al. Hepatocellular carcinoma: correlation between gadobenate dimeglumine-enhanced MRI and pathologic findings. Invest Radiol 2000;35:25–34.
18. Pirovano G, Vanzulli A, Marti-Bonmati L, et al. Evaluation of the accuracy of gadobenate dimeglumine-enhanced MR imaging in the detection and characterization of focal liver lesions. AJR Am J Roentgenol 2000;175:1111–1120.
19. Grazioli L, Kirchin MA, Pirovano G, Spinazzi A. MultiHance in the dynamic phase of contrast enhancement—a pictorial assessment. J Comput Assist Tomogr 1999;23(Suppl 1):S61–S64.
20. Petersein J, Spinazzi A, Giovagnoni A, et al. Evaluation of the efficacy of gadobenate dimeglumine in MR imaging of focal liver lesions: a multicenter phase III clinical study. Radiology 2000;215: 727–736.
21. Grazioli L, Morana G, Federle MP, et al. Focal nodular hyperplasia: morphological and functional information from MR imaging with gadobenate dimeglumine. Radiology 2001;221:731–739.
22. Mathieu D, Rahmouni A, Anglade MC, et al. Focal nodular hyperplasia of the liver: assessment with contrast-enhanced Turbo-FLASH MR imaging. Radiology 1991;180:25–30.
23. Grandin C, Van Beers BE, Robert A, Gigot J-F, Geubel A, Pringot J. Benign hepatocellular tumors: MRI after superparamagnetic iron oxide administration. J Comput Assist Tomogr 1995;19:412–418.
24. Beets-Tan RG, Van Engelshoven JMA, Greve JWM. Hepatic adenoma and focal nodular hyperplasia: MR findings with superparamagnetic iron oxide-enhanced MRI. Clin Imaging 1998;22:211–215.
25. Bismuth H. Surgical anatomy and anatomical surgery of the liver. World J Surg 1982;6:3–8.
26. Karhunen PJ. Benign hepatic tumours and tumour like conditions in men. J Clin Pathol 1986;9:183–188.
27. Itoh K, Saini S, Hahn PF, Imam N, Ferrucci JT. Differentiation between small hepatic hemangiomas and metastases on MR images. AJR Am J Roentgenol 1990;155:61–66.
28. Lombardo DM, Baker ME, Spritzer CE, Blinder R, Meyers W, Herfkens RJ. Hepatic hemangiomas vs metastases: hepatic differentiation at 1.5 T. AJR Am J Roentgenol 1990;155:55–59.
29. Brown JJ, Lee JM, Lee JKT, Van Lom KJ, Malchow SC. Focal MR lesions: differentiation with MR imaging at 0.5 T. Radiology 1991; 179:675–679.
30. Hamm B, Thoeni RF, Gould RG, et al. Focal liver lesions: characterization with nonenhanced and dynamic contrast material-enhanced MR imaging. Radiology 1994;190:417–423.
31. Semelka RC, Brown ED, Ascher SM, et al. Hepatic hemangiomas: a multi-institutional study of appearance of T2-weighted and serial gadolinium-enhanced gradient-echo MR images. Radiology 1994; 192:401–406.
32. Mitchell DG, Saini S, Weinreb J, et al. Hepatic metastases and cavernous hemangiomas: distinction with standard- and triple-dose gadoteridol-enhanced MR imaging. Radiology 1994;193:49–57.
33. Mahfouz AE, Hamm B, Wolf KJ. Peripheral washout: a sign of malignancy on dynamic gadolinium-enhanced MR images of focal liver lesions. Radiology 1994;190:49–52.
34. Nguyen BN, Flejou JF, Terris B, Belghiti J, Degott C. Focal nodular hyperplasia of the liver: a comprehensive pathologic study of 305 lesions and recognition of new histologic forms. Am J Surg Pathol 1999;23:1441–1454.
35. Choi CS, Freeny PC. Triphasic helical CT of hepatic focal nodular hyperplasia: incidence of atypical findings. AJR Am J Roentgenol 1998;170:391–395.
36. Carlson SK, Johnson CD, Bender CE, Welch TJ. CT of focal nodular hyperplasia of the liver. AJR Am J Roentgenol 2000;174:705–712.
37. Leese T, Farges O, Bismuth H. Liver cell adenomas. Ann Surg 1998;208:558–564.
38. Paley MR, Mergo PJ, Torres GM, Ros PR. Characterization of focal hepatic lesions with ferumoxides-enhanced T2-weighted MR imaging. AJR Am J Roentgenol 2000;175:159–163.
39. Pauleit D, Textor J, Bachmann R, et al. Hepatocellular carcinoma: detection with gadolinium- and ferumoxides-enhanced MR imaging of the liver. Radiology 2002;222:73–80.